Terahertz Response of Acoustically-Driven Optical Phonons

R. H. Poolman, E. A. Muljarov, and A. L. Ivanov

Department of Physics and Astronomy,

Cardiff University, Cardiff CF24 3AA, United Kingdom.

(Dated: April 12, 2010)

Abstract

The manipulation of TO-phonon polaritons and the terahertz (THz) light field associated with them by means of an ultra-sound acoustic wave is proposed and illustrated by calculating the TO-phonon-mediated THz response of acoustically-pumped CuCl and TlCl crystals. We show the high-contrast acoustically-induced change of the THz reflectivity alongside with multiple THz Bragg replicas, which are associated with the infrared-active TO-phonon resonance driven by the ultrasonic wave. The effect, which stems from phonon anharmonicity, refers to an operating acoustic intensity $I_{\rm ac} \sim 1 - 100\,{\rm kW/cm^2}$ and frequency $\nu_{\rm ac} \sim 0.1 - 1\,{\rm GHz}$, with possible applications in THz spectroscopy.

PACS numbers: 43.35.+d, 71.36.+c, 78.20.Pa

Since the pioneering work by Kun Huang [1], the physics of infrared polaritons associated with transverse optical (TO) phonons has emerged as a well-established discipline. Recently, room-temperature polaritonics was implemented for processing and coherent control of the THz light field [2, 3]. In addition to conventional infrared spectroscopy and continuous-wave Raman scattering experiments, broadband THz time-domain spectroscopy has been developed and successfully applied to characterize picosecond (ps) and sub-ps dynamics of infrared-active TO-phonons [4] and to visualize the polariton dispersion associated with these vibrational modes [5]. Furthermore, the THz polariton spectra allow to study unusual lattice dynamics, e.g., in ferroelectrics [6] and negative thermal expansion compounds [7, 8]. However, the spectrally-resolved control of the THz electromagnetic field associated with infrared polaritons still remains a very challenging task of far-infrared spectroscopy.

In this Letter we propose an acoustic modulation of TO-phonon polaritons to drastically change their optical response in the THz band. Phonon anharmonicity, which can be large in some dielectric and semiconductor materials and particularly strong for soft TO-phonon modes, leads to the coupling between a coherent (pumping) acoustic wave (AW) and infrared-active TO-phonons. In this case one deals with an *acoustically-induced Autler-Townes effect*, which gives rise to spectral gaps Δ_N in the THz polariton spectrum of AW-driven TO-phonons, and is akin to the acoustical Stark effect for excitons [9]. The AW-induced gaps Δ_N, which open up in the polariton spectrum and develop with increasing acoustic intensity $I_{\rm ac}$, are due to the Nth-order resonant acoustic phonon transitions within the polariton dispersion branches. These forbidden-energy gaps strongly modify the optical response of TO-phonon polaritons and make possible the effective AW manipulation of the THz field.

The spectrally-resolved AW control of the THz field propagation can also be interpreted in terms of Bragg diffraction of infrared polaritons by the pumping AW: For the first time we analyze the use of phonon anaharmonicity to create an acoustically-induced Bragg grating. In this case the contrast of the AW grating is dictated by the efficiency of the scattering channel "TO-phonon $\pm$ acoustic phonon (two acoustic phonons) $\leftrightarrow$ TO-phonon" for cubic (quartic) phonon anharmonicity. Thus the scattering of THz light is mediated and strongly enhanced by the TO-phonon resonance. This results in an anomalously short interaction length needed for formation of the Bragg replicas. Possible applications of governing infrared polaritons by using an ultrasonic acoustic field include frequency-tunable THz detectors and filters, Bragg switchers and frequency converters.

The Hamiltonian of infrared polaritons coherently driven by a cw bulk acoustic wave $\{\mathbf{k}, \omega_{\rm ac}(k)\}$ is given by

$$H = H_0 + \sum_{\mathbf{p}} \Big[2\tilde{m}_4 I_{\rm ac} b^\dagger_{\mathbf{p}} b_{\mathbf{p}} \; + \; \left(m_3 I_{\rm ac}^{1/2} e^{-i\omega_{\rm ac} t} b^\dagger_{\mathbf{p}} b_{\mathbf{p}-\mathbf{k}} + \text{H. c.} \right) \\ + \; \left(m_4 I_{\rm ac} e^{-2i\omega_{\rm ac} t} b^\dagger_{\mathbf{p}} b_{\mathbf{p}-2\mathbf{k}} + \text{H. c.} \right) \Big] , \tag{1}$$

with H_0 the conventional polariton Hamiltonian of infrared-active TO-phonons [10], $b_{\mathbf{p}}$ the TO-phonon operator, $\omega_{\rm ac} = 2\pi\nu_{\rm ac} = v_{\rm s} k$, $v_{\rm s}$ the sound velocity, and m_3 (m_4 and $\tilde{m}_4$) the matrix element associated with cubic (quartic) anharmonicity. The macroscopic equations, which describe the control of THz polaritons by applying the acoustic field of an arbitrary profile, $I_{\rm ac} = I_{\rm ac}(\mathbf{r}, t)$, are

$$\left[\frac{\varepsilon_{\rm b}}{c^2} \frac{\partial^2}{\partial t^2} - \nabla^2 \right] \mathbf{E}(\mathbf{r}, t) = -\frac{4\pi}{c^2} \frac{\partial^2}{\partial t^2} \mathbf{P}(\mathbf{r}, t) \, , \tag{2}$$

$$\Big[\frac{\partial^2}{\partial t^2} + 2\gamma_{\rm TO} \frac{\partial}{\partial t} + \Omega_{\rm TO}^2 + 4\Omega_{\rm TO} \tilde{m}_4 I_{\rm ac}(\mathbf{r}, t) + 4\Omega_{\rm TO} m_3 I_{\rm ac}^{1/2}(\mathbf{r}, t) \cos(\omega_{\rm ac} t - \mathbf{kr}) \\ + \; 4\Omega_{\rm TO} m_4 I_{\rm ac}(\mathbf{r}, t) \cos(2\omega_{\rm ac} t - 2\mathbf{kr}) \Big] \mathbf{P}(\mathbf{r}, t) = \frac{\varepsilon_{\rm b}}{4\pi} \Omega_{\rm R}^2 \, \mathbf{E}(\mathbf{r}, t) \, , \tag{3}$$

where $\mathbf{E}$ and $\mathbf{P}$ stand for the light field and TO-phonon polarization, respectively, $\Omega_{\rm TO}$ is the TO-phonon frequency, $\Omega_{\rm R}$ is the polariton Rabi frequency, $\varepsilon_{\rm b}$ is the background dielectric constant in the infrared, and $\gamma_{\rm TO}$ is the damping rate of TO-phonons, mainly due to their decay into short-wavelength acoustic phonons. Equations (2)-(3) refer to simple cubic lattices with spatially isotropic long-wavelength anharmonicity and optical response. For cw acoustic excitations, when $I_{\rm ac}(\mathbf{r}, t) = I_{\rm ac} = \text{const.}$, Eqs. (2)-(3) yield the same quasi-energy spectrum as that of the quadratic Hamiltonian (1). If $I_{\rm ac} = 0$, Eqs. (2)-(3) reduce to the standard TO-phonon polariton equations [1]. The forth term on the left-hand side (l.h.s.) of the polarization Eq. (3) yields a Stark shift of the TO-phonon frequency, which is $\propto I_{\rm ac}$ and is associated with the quartic phonon nonlinearity. The last two terms on the l.h.s. of Eq. (3) give rise to the Bragg spectrum of TO-phonon polaritons driven by the AW.

The matrix elements associated with cubic and quartic anharmonicity are $m_3 = 6[v_0/(\hbar^3 v_{\rm s}^2 k)]^{1/2} V_3(\mathbf{k}, \mathbf{p}-\mathbf{k}, -\mathbf{p})$, $m_4 = 12[v_0/(\hbar^2 v_{\rm s}^2 k)][V_4(\mathbf{k}, \mathbf{k}, \mathbf{p}-2\mathbf{k}, -\mathbf{p}) + V_4(\mathbf{k}, \mathbf{k}, -\mathbf{p}, \mathbf{p}-2\mathbf{k})]$, and $\tilde{m}_4 = 24[v_0/(\hbar^2 v_{\rm s}^2 k)] V_4(\mathbf{k}, -\mathbf{k}, \mathbf{p}, -\mathbf{p})$, with v_0 a volume of the primitive cell. The potential V_3 is given by $V_3(\mathbf{k}, \mathbf{p}-\mathbf{k}, -\mathbf{p}) = (1/6)[\hbar^3/(8\omega_{\rm ac}\Omega_{\rm TO}^2)]^{1/2} \Phi^{(3)}(\mathbf{k}, \mathbf{p}-\mathbf{k}, -\mathbf{p})$, where $\Phi^{(3)}$ is proportional to the Fourier transform of the third-order derivative of the interatomic

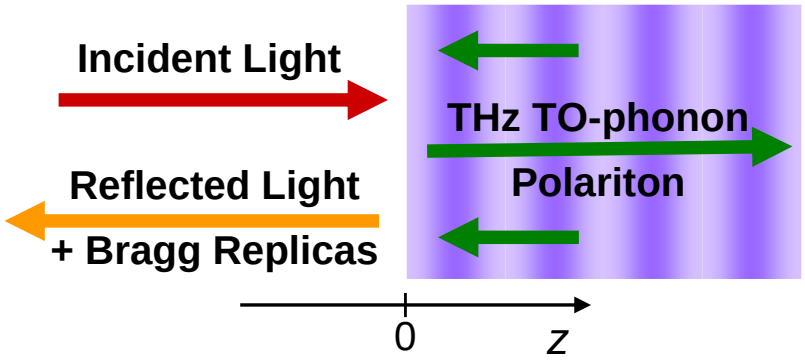

FIG. 1: (Color online) Schematic of optical excitation and backward Bragg scattering of an acoustically-driven THz polariton. Vertical stripes symbolize the propagating bulk acoustic wave.

potential. There is a similar expression for the forth-order potential, $V_4 \propto \Phi^{(4)}$ (the explicit formulae for $V_{3,4}$ and $\Phi^{(3,4)}$ are given, e.g., in Refs. [11, 12]). In the long-wavelength limit $k, p \ll 1/a_0$ (a_0 is the lattice constant), relevant to the optics of TO-phonon polaritons, $\Phi^{(3,4)}$ are well-approximated by $\Phi^{(3)} = (ka_0)C_3$ and $\Phi^{(4)} = (ka_0)^2 C_4$ [13]. The anharmonicity constants $C_{3,4}$ can either be calculated by using modern *ab initio* methods [14, 15] or evaluated from experimental data available for some anharmonic crystals [16–18]. The above approximation of $\Phi^{(3,4)}$ also leads to the k-independent matrix elements m_3 and $\tilde{m}_4 = m_4$ in Eqs. (1) and (3).

Recently, the third-order coupling constant V_3 was inferred for some zincblende-type semiconductors (GaP, CuCl, CuBr, and β-ZnS) which exhibit strong and dominant cubic anharmonicity [16, 17]. The used experimental data refers to the decay of a long-wavelength TO-phonon into short-wavelength longitudinal (LA) and transverse (TA) acoustic phonons. To adapt the inferred values of V_3 to m_3 in Eq. (1) and Eqs. (2)-(3), we use the Leibfried-Ludwig approximation [19]. The parameter $m_3 I_{\rm ac}^{1/2}$, which controls cubic-anharmonicity-mediated manipulation of THz polaritons by means of a bulk TA wave, is evaluated for CuCl as $m_3 I_{\rm ac}^{1/2} \simeq 0.26\,\text{meV}$ (63 GHz) for $I_{\rm ac} = 1\,\text{kW/cm}^2$. In thallium halides (TlCl and TlBr), quartic anharmonicity is dominant with positive values of V_4. With the Leibfried-Ludwig approximation, one can evaluate the control parameter $m_4 I_{\rm ac}$ from the available experimental data on the real part of the TO-phonon self-energy [18]. For TlCl driven by a bulk TA wave we get $m_4 I_{\rm ac} \simeq 0.4\,\text{meV}$ (97 GHz) for $I_{\rm ac} = 100\,\text{kW/cm}^2$. Note that m_3 and m_4 scale to the sound velocity as $v_{\rm s}^{-3/2}$ and $v_{\rm s}^{-3}$, respectively, so that the use of surface AWs considerably reduces the operating acoustic intensity.

We examine the optical response of an acoustically-driven TO-phonon polariton in a one-dimensional geometry, when a semiconductor occupies the half space $z > 0$, and a normally incident light field of frequency ω induces a THz polariton propagating collinearly to the pumping AW (see Fig. 1). In this case, apart from reflectivity at the same frequency ω, down-converted Bragg replicas at $\omega + n\omega_{\rm ac}$ ($n = -1, -2, ...$) arise in the reflection spectrum, due to acoustically-induced backward scattering of the polariton. In order to calculate the multiple Bragg replicas, we develop an approach more advanced than that used in conventional acousto-optics. For the latter, the acousto-optical susceptibilities are so weak that usually only one Bragg replica $n = +1$ or -1 is seen. In contrast, the TO-phonon resonance mediates and considerably enhances the coupling between the optical and acoustic fields, so that generally one has to take into account the whole series of the Bragg replicas and multi-phonon transitions, thus treating the problem non-perturbatively.

The quasi-energy polariton spectrum $\omega = \omega(p)$, calculated for real-valued p (quasiparticle solution) by solving Eqs. (2)-(3) with $m_4 = 0$, is plotted in Fig. 2 (a) for CuCl parametrically driven by the TA wave of frequency $\nu_{\rm ac} = 50\,{\rm MHz}$ and constant intensity $I_{\rm ac} = 25\,{\rm kW/cm^2}$. The spectrum, which arises from spatial and temporal modulation of the crystal lattice, can be interpreted in terms of the Brillouin zone picture, with acoustically-induced energy gaps $\Delta_N \propto I_{\rm ac}^{N/2}$ due to the N-phonon resonant transitions within the polariton dispersion branches. The spectral positions of the transitions are indicated in Fig. 2 (a) by the vertical arrows. For the frequency scale used in Fig. 2 (a), only the gaps $\Delta_{N=1}$ and $\Delta_{N=2}$ in the upper polariton branch are clearly seen.

From the air side, $z < 0$ (see Fig. 1), the light field is given by

$$E(z < 0, t) = e^{iq_0 z} e^{-i\omega t} + \sum_n r_n e^{-iq_n z} e^{-i(\omega + n\omega_{\rm ac})t}\,, \tag{4}$$

where $q_n = (\omega + n\omega_{\rm ac})/c$ with $-n_{\rm max} \leqslant n \leqslant n_{\rm max}$ (we proceed up to $n_{\rm max} = 60$) and r_n stands for the amplitude of the outgoing Bragg replica n normalized to the unity amplitude of the incoming light wave. The electric field propagating in the crystal ($z > 0$) is

$$E(z > 0, t) = \sum_{n,j} A_j E_{nj} e^{i(p_j + nk)z - i(\omega + n\omega_{\rm ac})t}\,. \tag{5}$$

Here, $p_j = p_j(\omega)$ is the wavevector associated with the quasi-energy dispersion branch j ($n_{\rm max} \leqslant j \leqslant n_{\rm max}$) of the acoustically-driven polariton, E_{nj} are the corresponding normalized eigenvectors, and A_j are the eigenmode amplitudes. Both $p_j = p_j(\omega)$ and E_{nj} are the

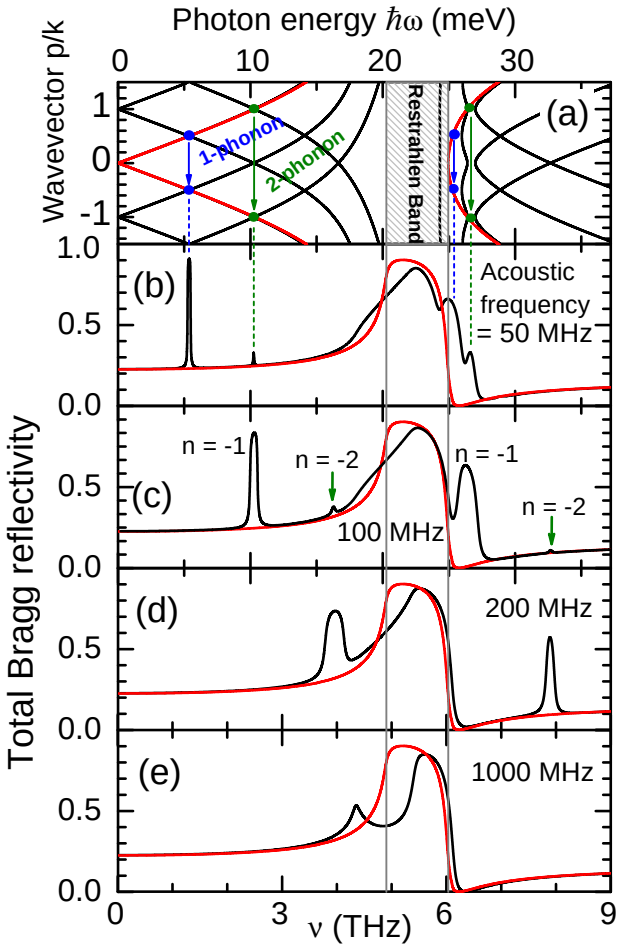

FIG. 2: (Color online) (a) The dispersion $\omega = \omega(p)$ of THz polaritons in CuCl driven by the bulk TA-wave of $\nu_{\rm ac} = 50\,{\rm MHz}$ (black lines) and the bare polariton spectrum (red lines). The wavevector p is normalized to the acoustic wavevector k. The arrows highlight the N-TA-phonon resonant coupling between the polariton states ($N = 1, 2$). (b)-(e) The calculated total Bragg reflectivity (black lines), $R = \sum_n |r_n|^2$, against the light frequency $\nu = \omega/(2\pi)$ for $\nu_{\rm ac} = 50\,{\rm MHz}$, 100 MHz, 200 MHz, and 1 GHz, respectively. The bare polariton reflectivity is shown by the red lines. The Bragg signals labelled in (c) as $n = -1$ and $n = -2$ are mainly due to $|r_{-1}|^2$ and $|r_{-2}|^2$, respectively. $I_{\rm ac} = 25\,{\rm kW/cm^2}$, $\hbar\Omega_{\rm TO} = 20.28\,{\rm meV}$, $\hbar\Omega_{\rm R} = 14.53\,{\rm meV}$, and $\hbar\gamma_{\rm TO} = 0.2\,{\rm meV}$.

forced-harmonic solutions of Eqs. (2)-(3) for real-valued frequency ω. The exponential on the r.h.s. of Eq. (5) as well as the basic relationships $p_{j+s}(\omega) = p_j(\omega - s\omega_{\rm ac}) + sk$ and $E_{n,j+s}(\omega) = E_{n+s,j}(\omega - s\omega_{\rm ac})$, with integer s, reflect the acoustic wavevector and frequency translational invariance of the quasi-energy spectrum. The Maxwellian boundary conditions

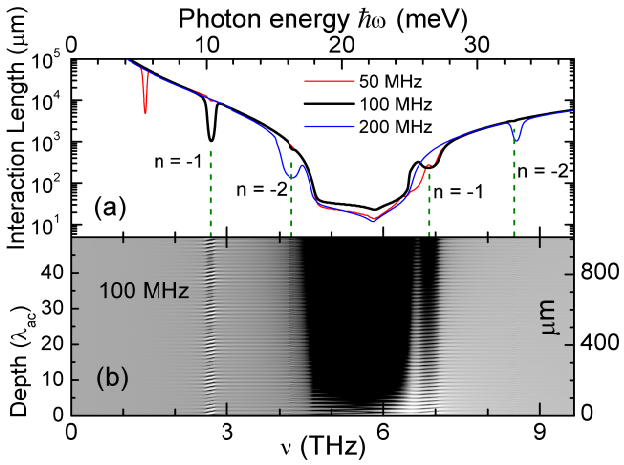

FIG. 3: (Color online) (a) The interaction length between the THz polariton and TA pumping wave in CuCl, $\ell_{\rm int} = \ell_{\rm int}(\omega)$, calculated for $I_{\rm ac} = 25\,{\rm kW/cm^2}$ and $\nu_{\rm ac} = 50\,{\rm MHz}$, $100\,{\rm MHz}$, and $200\,{\rm MHz}$. (b) The electric field profile $|E(z>0,\omega)|^2$ evaluated for $\nu_{\rm ac} = 100\,{\rm MHz}$ ($\lambda_{\rm ac} = 20.2\,\mu{\rm m}$). The color scale is logarithmic with black color corresponding to $E \to 0$.

at $z = 0$ together with Eqs. (4)-(5) yield:

$$\delta_{n,0} + r_n = \sum_j A_j E_{nj}\,, \qquad \delta_{n,0} - r_n = \sum_j A_j E_{nj} \frac{p_j + nk}{q_n}\,. \tag{6}$$

The set of $2(2n_{\rm max}+1)$ linear Eqs. (6) determines r_n and A_j.

In Figs. 2 (b)-(e) we compare the calculated total Bragg reflectivity, $R = R(\omega) = \sum_n |r_n|^2$ (black solid lines), with the reflectivity of the acoustically unperturbed THz polariton, $R^{(0)} = R^{(0)}(\omega)$ (red solid lines). The sharp spikes in the Bragg spectrum of the acoustically-driven CuCl crystal are clearly seen for the one-TA-phonon and two-TA-phonon transitions, both for the upper (UP) and lower (LP) polariton branches [see Fig. 2 (a) against Fig. 2 (b)]. For $\nu_{\rm ac} \sim 30 - 300\,{\rm MHz}$, the backward scattered Bragg replica $|r_{-1}|^2$ peaks at the energy of the one-phonon transition and is highly efficient, with $|r_{-1}|^2/R \sim 50\,\% - 70\,\%$. The peak position and its strength are effectively tunable by changing the frequency and intensity of the AW [see Figs. 2 (b)-(d)]. This can be used for the frequency down-conversion by $\omega_{\rm ac} = 2\pi\nu_{\rm ac}$ of the optically-induced THz polariton and of the incident light field. Generally, the backward Bragg scattering signals $|r_n|^2 \propto I_{\rm ac}^{|n|}$ ($n < 0$) peak at the spectral position of the gaps $\Delta_{N\leqslant|n|}$, i.e., for the light frequency $\omega = \omega_N$ which satisfies the resonant Bragg condition $p_{j=0}(\omega_N) \simeq Nk/2$ with $N = 1, 2, .., |n|$.

The Bragg signal $n = 0$ appears as the AW-induced change of the reflectivity at incident

frequency ω, $|r_0(\omega)|^2 - R^{(0)}(\omega)$. The strength of the $n = 0$ signal sharply increases with decreasing detuning $|\omega - \Omega_{\rm TO}|$ from the TO-phonon resonance, so that $|r_0|^2 - R^{(0)}$ becomes dominant over $|r_{-1}|^2$. For $\nu_{\rm ac} \gtrsim 1\,{\rm GHz}$, when the one-acoustic-phonon transition within the LP branches occurs very close to $\Omega_{\rm TO}$, the AW-induced change of the reflectivity [see Fig. 2 (e)] is completely determined by the $n = 0$ replica and has no $\nu_{\rm ac}$-down-converted frequency components. Thus this operating mode can be used for TO-phonon polariton deflectors and acoustically-controlled THz filters.

The interaction length $\ell_{\rm int} = \ell_{\rm int}(\omega)$ required for the formation of the Bragg signals and thus for AW control of the THz light field is plotted in Fig. 3 (a) for various $\nu_{\rm ac}$. The sharp troughs at $\omega = \omega_{N=1}$ and $\omega_{N=2}$ in the $\ell_{\rm int} = \ell_{\rm int}(\omega)$ profile are due to the $n = -1$ and -2 Bragg replicas [see Fig. 3 (a)]. Figure 3 (b) shows the light field distribution associated with the optically-induced THz polariton in the acoustically-driven CuCl crystal. Apart from the broad black band [see Fig. 3 (b)], which corresponds to the Restrahlen band with rather weak penetration of the light field into the crystal, the narrow stripes of alternating color illustrate the formation of the Bragg replicas. The interaction length for the $n = -1$ replica at its resonant frequency $\omega = \omega_{N=1}$ is given by

$$\ell_{\rm int} = \frac{\hbar k c^2}{4 m_3 I_{\rm ac}^{1/2} \varepsilon_{\rm b}} \frac{(\omega_{N=1}^2 - \Omega_{\rm TO}^2)^2}{\omega_{N=1}^2 \Omega_{\rm TO} \Omega_{\rm R}^2}\,. \tag{7}$$

Equation (7), which is valid for $|\Omega_{\rm TO} - \omega_{N=1}| \gg \gamma_{\rm TO}$ and $\ell_{\rm int} k \gg 1$, shows the resonant decrease of $\ell_{\rm int} \propto 1/\sqrt{I_{\rm ac}}$ with decreasing frequency detuning from the TO-phonon resonance. In this case the interaction between the light field and pumping AW is mediated by the TO-phonon resonance, giving rise to $\ell_{\rm int}$ of only a few tens of acoustic wavelength $\lambda_{\rm ac}$ (see Fig. 3). This is in sharp contrasts with conventional acousto-optics where $\ell_{\rm int} \sim 10^3 - 10^4\,\lambda_{\rm ac}$ for the same operating $I_{\rm ac}$.

Within the used nonperturbative approach, each Bragg replica n integrates all $n + s - s$ TA-phonon transitions with $s \leqslant n_{\rm max}$: With increasing $I_{\rm ac}$ the bare n-phonon transitions become dressed by higher-order processes when $n + s$ phonons are emitted and s phonons absorbed. For the $n = -1$ replica shown in Fig. 2 (b), e.g., the multiphonon transitions $-1+1-1$, $-1+2-2$, etc. account for about 90 % of $|r_{-1}|^2$. For $\nu_{\rm ac} \gtrsim 1\,{\rm GHz}$, the dominant contribution to $|r_0|^2 - R^{(0)}$ stems from $-s + s$ multi-TA-phonon transitions with $s > 1$.

The calculated room temperature reflectivity $R = R(\omega)$ of a TlCl crystal driven by the TA wave of frequency $\nu_{\rm ac} = 25\,{\rm MHz}$ and $125\,{\rm MHz}$ is plotted in Figs. 4 (a) and (b), respectively.

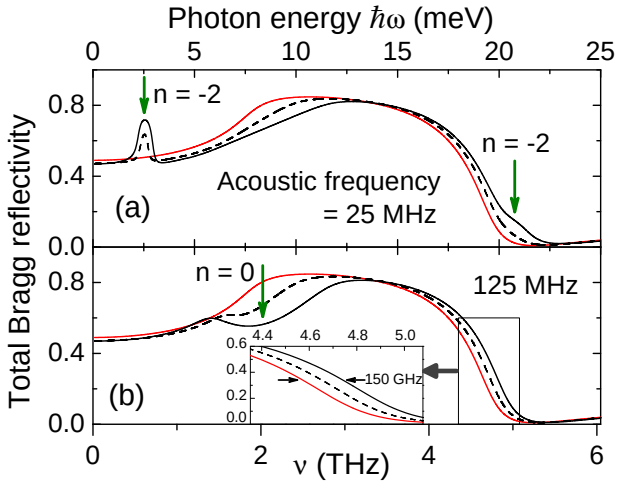

FIG. 4: (Color online) The total Bragg reflectivity $R = R(\omega)$ of a TlCl crystal driven by the TA wave of frequency $\nu_{\rm ac} = 25\,$MHz (a) and 125 MHz (b), $I_{\rm ac} = 100\,{\rm kW/cm^2}$ (black dotted lines) and $200\,{\rm kW/cm^2}$ (black solid lines). The acoustically-unperturbed THz spectrum $R^{(0)} = R^{(0)}(\omega)$ is shown by the red lines. Insert: The acoustically-induced Stark shift of the TO-phonon line. $\hbar\Omega_{\rm TO} = 7.81\,$meV, $\hbar\Omega_{\rm R} = 17.97\,$meV, and $\hbar\gamma_{\rm TO} = 0.92\,$meV.

In this case, in Eqs. (1) and (3) we put $m_3 = 0$, and only even-order TA-phonon-assisted transitions occur. The Bragg signals $n = -2$, due to $|r_{-2}|^2 \propto I_{\rm ac}^2$, are indicated in Fig. 4 (a) by arrows, for the transitions within the LP and UP branches, respectively. Similarly to the previous case (CuCl), for THz light frequency ω close to $\Omega_{\rm TO}$ the AW-induced change of R, $\Delta R = R - R^{(0)} \sim I_{\rm ac}^2$ [see Fig. 4 (b)], is mainly due to the $n = 0$ Bragg replica. The quartic nonlinearity leads to the Stark blue shift by $2m_4 I_{\rm ac}$ of the TO-phonon frequency, according to Eqs. (1) and (3), as is clearly seen in Figs. 4 (a) and (b). The Stark shift $\sim 0.1 - 0.2\,$THz has a rather sharp contrast on the blue side of the THz reflectivity [see inset in Fig. 4 (b)].

The acoustically-induced modulation of infrared polaritons has to be particularly strong for ferroelectric soft TO-phonons (e.g., in $LiTaO_3$ and $LiNbO_3$ [6] and bismuth titanate [5]). In this case, a multi-well local potential for the displacive ferroelectric mode has a considerable low-wavevector component and therefore yields large values of V_3 and V_4. Far-infrared optical phonons ($2-10\,$meV) in zirconium tungstate (ZrW_2O_8) indicate anomalously high anharmonicity [7, 8]. The normal modes associated with soft TO-phonons in this negative thermal expansion compound are a mixture of librational and translational motion. The latter strongly couples with acoustic phonons giving rise, as we foresee, to manipulation of the THz polaritons by using utrasound waves of modest $I_{\rm ac}$.

We thank S. G. Tikhodeev and R. Zimmermann for valuable discussions. This work was supported by RS (Grant JP0766306), EPSRC and WIMCS.

[1] K. Huang, Nature **167**, 779 (1951); Proc. Roy. Soc. A **208**, 352 (1951).

[2] N. S. Stoyanov *et al.*, Nature Materials **1**, 95 (2002).

[3] T. Feurer, J. C. Vaughan, and K. A. Nelson, Science **299**, 374 (2003).

[4] P. Y. Han and X.-C. Zhang, Meas. Sci. Technol. **12**, 1747 (2001).

[5] S. Kojima *et al.*, Phys. Rev. B **67**, 035102 (2003).

[6] H. J. Bakker, S. Hunsche, and H. Kurz, Rev. Mod. Phys. **70**, 523 (1998).

[7] J. N. Hancock *et al.* Phys. Rev. Lett. **93**, 225501 (2004).

[8] S. L. Chaplot, Curr. Sci. **88**, 347 (2005).

[9] A. L. Ivanov and P. B. Littlewood, Phys. Rev. Lett. **87**, 136403 (2001); K. Cho *et al.*, ibid **94**, 226406 (2005); M. M. de Lima *et al.*, ibid **97**, 045501 (2006).

[10] V. Romero-Rochin *et al.*, J. Chem. Phys. **111**, 3559 (1999).

[11] A. A. Maradudin and A. E. Fein, Phys. Rev. **128**, 2589 (1962).

[12] R. A. Cowley, Rep. Prog. Phys. **31**, 123 (1968).

[13] G. P. Srivastava, *The Physics of Phonons* (Taylor & Francis Group, New York, 1990).

[14] A. Debernardi, S. Baroni, and E. Molinari, Phys. Rev. Lett. **75**, 1819 (1995).

[15] G. Deinzer *et al.*, Phys. Rev. B **69**, 014304 (2004).

[16] C. Ulrich *et al.*, Phys. Rev. Lett. **82**, 351 (1999); F. Widulle *et al.*, ibid **82**, 5281 (1999); J. Serrano *et al.*, Phys. Rev. B **69**, 014301 (2004).

[17] M. Cardona and T. Ruf, Solid State Commun. **117**, 201 (2001).

[18] R. P. Lowndes, Phys. Rev. Lett. **27**, 1134 (1971); Phys. Rev. B **6**, 1490 (1972).

[19] G. Leibfried and W. Ludwig, in *Solid State Physics* **12**, Eds. F. Seitz and D. Turnbull (Academic Press, New York, 1961).